

A low-power high-speed InP microdisk modulator heterogeneously integrated on a SOI waveguide

Jens Hofrichter,^{1,*} Oded Raz,² Antonio La Porta,¹ Thomas Morf,¹ Pauline Mechet,³ Geert Morthier,³ Tjibbe De Vries,² Harm J. S. Dorren,² and Bert J. Offrein¹

¹IBM Research – Zurich, Säumerstrasse 4, 8803 Rüschlikon, Switzerland

²COBRA Research Institute, Eindhoven University of Technology, Eindhoven, P.O. Box 513, 5600 MB, The Netherlands

³INTEC, Ghent University—IMEC, St-Pietersnieuwstraat 41, 9000 Ghent, Belgium
[*jho@zurich.ibm.com](mailto:jho@zurich.ibm.com)

Abstract: We report on the modulation characteristics of indium phosphide (InP) based microdisks heterogeneously integrated on a silicon-on-insulator (SOI) waveguide. We present static extinction ratios and dynamic operation up to 10 Gb/s. Operation with a bit-error rate below 1×10^{-9} is demonstrated at 2.5, 5.0 and 10.0 Gb/s and the performance is compared with that of a commercial modulator. Power penalties are analyzed with respect to the pattern length. The power consumption is calculated and compared with state-of-the-art integrated modulator concepts. We demonstrate that InP microdisk modulators combine low-power and low-voltage operation with low footprint and high-speed. Moreover, the devices can be fabricated using the same technology as for lasers, detectors and wavelength converters, making them very attractive for co-integration.

©2012 Optical Society of America

OCIS codes: (130.4110) Modulators; (130.3120) Integrated optics devices; (230.4110) Modulators; (230.4205) Multiple quantum well (MQW) modulators; (250.4110) Modulators.

References and links

1. I. Christiaens, G. Roelkens, K. De Mesel, D. Van Thourhout, and R. Baets, "Adhesive wafer bonding with Benzocyclobutene," *J. Lightwave Technol.* **1**(11), 1–7 (2004).
2. G. Roelkens, J. Brouckaert, D. Taillaert, P. Dumon, W. Bogaerts, D. Van Thourhout, R. Baets, R. Nötzel, and M. Smit, "Integration of InP/InGaAsP photodetectors onto silicon-on-insulator waveguide circuits," *Opt. Express* **13**(25), 10102–10108 (2005).
3. H. Park, Y. H. Kuo, A. W. Fang, R. Jones, O. Cohen, M. J. Paniccia, and J. E. Bowers, "A hybrid AlGaInAs-silicon evanescent preamplifier and photodetector," *Opt. Express* **15**(21), 13539–13546 (2007).
4. J. Van Campenhout, P. Rojo Romeo, P. Regreny, C. Seassal, D. Van Thourhout, S. Verstuyft, L. Di Cioccio, J.-M. Fedeli, C. Lagahe, and R. Baets, "Electrically pumped InP-based microdisk lasers integrated with a nanophotonic silicon-on-insulator waveguide circuit," *Opt. Express* **15**(11), 6744–6749 (2007).
5. A. W. Fang, H. Park, O. Cohen, R. Jones, M. J. Paniccia, and J. E. Bowers, "Electrically pumped hybrid AlGaInAs-silicon evanescent laser," *Opt. Express* **14**(20), 9203–9210 (2006).
6. X. K. Sun, A. Zadok, M. J. Shearn, K. A. Diest, A. Ghaffari, H. A. Atwater, A. Scherer, and A. Yariv, "Electrically pumped hybrid evanescent Si/InGaAsP lasers," *Opt. Lett.* **34**(9), 1345–1347 (2009).
7. L. Liu, J. Van Campenhout, G. Roelkens, D. Van Thourhout, P. Rojo Romeo, P. Regreny, C. Seassal, J.-M. Fédéli, and R. Baets, "Ultralow-power all-optical wavelength conversion in a silicon-on-insulator waveguide based on a heterogeneously integrated III–V microdisk laser," *Appl. Phys. Lett.* **93**(6), 061107 (2008).
8. O. Raz, L. Liu, D. Van Thourhout, P. Rojo-Romeo, J.-M. Fédéli, and H. J. S. Dorren, "High speed wavelength conversion in a heterogeneously integrated disk laser over silicon on insulator for network on a chip applications," presented at the 35th European Conference on Optical Communication (ECOC 2009), Paper 4.2.3, Vienna, Austria, Sept. 2009.
9. J. Hofrichter, O. Raz, L. Liu, G. Morthier, F. Horst, P. Regreny, T. De Vries, H. J. S. Dorren, and B. J. Offrein, "All-optical wavelength conversion using mode switching in InP microdisc laser," *Electron. Lett.* **47**(16), 927–929 (2011).
10. L. Liu, J. Van Campenhout, G. Roelkens, R. A. Soref, D. Van Thourhout, P. Rojo-Romeo, P. Regreny, C. Seassal, J.-M. Fédéli, and R. Baets, "Carrier-injection-based electro-optic modulator on silicon-on-insulator with a heterogeneously integrated III-V microdisk cavity," *Opt. Lett.* **33**(21), 2518–2520 (2008).

11. Y.-H. Kuo, H.-W. Chen, and J. E. Bowers, "High speed hybrid silicon evanescent electroabsorption modulator," *Opt. Express* **16**(13), 9936–9941 (2008).
12. M. R. Watts, D. C. Trotter, R. W. Young, and A. L. Lentine, "Ultralow power silicon microdisk modulators and switches," in *Proc. 5th IEEE Int'l Conf. Group IV Photonics*, Sorrento, Italy, Sept. 2008, pp. 4–6. <http://ieeexplore.ieee.org/stamp/stamp.jsp?tp=&arnumber=4638077>.
13. Q. Xu, S. Manipatruni, B. Schmidt, J. Shakya, and M. Lipson, "12.5 Gbit/s carrier-injection-based silicon micro-ring silicon modulators," *Opt. Express* **15**(2), 430–436 (2007).
14. W. M. Green, M. J. Rooks, L. Sekaric, and Y. A. Vlasov, "Ultra-compact, low RF power, 10 Gb/s silicon Mach-Zehnder modulator," *Opt. Express* **15**(25), 17106–17113 (2007).
15. J. E. Roth, O. Fidaner, R. K. Schaevitz, Y.-H. Kuo, T. I. Kamins, J. S. Harris, Jr., and D. A. B. Miller, "Optical modulator on silicon employing germanium quantum wells," *Opt. Express* **15**(9), 5851–5859 (2007).
16. J. Liu, M. Beals, A. Pomerene, S. Bernardis, R. Sun, J. Cheng, L. C. Kimerling, and J. Michel, "Waveguide-integrated ultralow-energy GeSi electro-absorption modulators," *Nat. Photonics* **2**(7), 433–437 (2008).
17. P. Dumon, W. Bogaerts, V. Wiaux, J. Wouters, S. Beckx, J. Van Campenhout, D. Taillaert, B. Luysaert, P. Bienstman, D. Van Thourhout, and R. Baets, "Low-loss SOI Photonic Wires and Ring Resonators Fabricated with Deep UV Lithography," *IEEE Photon. Technol. Lett.* **16**(5), 1328–1330 (2004).
18. J. Boucart, C. Starck, F. Gaborit, A. Plais, N. Bouche, E. Derouin, J. C. Remy, J. Bonnet-Gamard, L. Goldstein, C. Fortin, D. Carpentier, P. Salet, F. Brillouet, and J. Jacquet, "Metamorphic DBR and Tunnel-Junction Injection L A CW RT Monolithic Long-Wavelength VCSEL," *IEEE J. Sel. Top. Quantum Electron.* **5**(3), 520–529 (1999).
19. M. N. Sysak, J. O. Anthes, J. E. Bowers, O. Rada, and R. Jones, "Integration of hybrid silicon lasers and electroabsorption modulators," *Opt. Express* **16**(17), 12478–12486 (2008).
20. IBM. Microelectronics Specialty Foundry Selection Guide, downloadable from: <http://public.dhe.ibm.com/common/ssi/ecm/en/tgb03009usen/TGB03009USEN.PDF>
21. O. Mitomi, S. Nojima, I. Kotaka, K. Wakita, K. Kawano, and M. Naganuma, "Chirping Characteristic and Frequency Response of MQW Optical Intensity Modulator," *J. Lightwave Technol.* **10**(1), 71–77 (1992).
22. G. Agrawal, *Fiber-Optic Communication Systems* (New York, John Wiley & Sons, 1997).
23. M. R. Watts, W. A. Zortman, D. C. Trotter, R. W. Young, and A. L. Lentine, "Vertical junction silicon microdisk modulators and switches," *Opt. Express* **19**(22), 21989–22003 (2011).
24. P. Dong, S. Liao, D. Feng, H. Liang, D. Zheng, R. Shafiiha, C.-C. Kung, W. Qian, G. Li, X. Zheng, A. V. Krishnamoorthy, and M. Asghari, "Low V_{pp} , ultralow-energy, compact, high-speed silicon electro-optic modulator," *Opt. Express* **17**(25), 22484–22490 (2009).
25. P. Dong, S. Liao, H. Liang, W. Qian, X. Wang, R. Shafiiha, D. Feng, G. Li, X. Zheng, A. V. Krishnamoorthy, and M. Asghari, "High-speed and compact silicon modulator based on a racetrack resonator with a 1 V drive voltage," *Opt. Lett.* **35**(19), 3246–3248 (2010).
26. A. S. Liu, R. Jones, L. Liao, D. Samara-Rubio, D. Rubin, O. Cohen, R. Nicolaescu, and M. Paniccia, "A high-speed silicon optical modulator based on a metal-oxide-semiconductor capacitor," *Nature* **427**(6975), 615–618 (2004).
27. D. Marris-Morini, X. Le Roux, L. Vivien, E. Cassan, D. Pascal, M. Halbwx, S. Maine, S. Laval, J. M. Fédéli, and J. F. Damlencourt, "Optical modulation by carrier depletion in a silicon PIN diode," *Opt. Express* **14**(22), 10838–10843 (2006).

1. Introduction

Silicon photonics is a promising technology platform that is expected to deliver the ever more demanding input-output (IO) bandwidth and density required in future computing systems. However, as silicon itself does not exhibit electrically pumped optical gain due to its indirect band structure, heterogeneous integration is an attractive path to extend the capabilities of silicon photonics [1]. Using heterogeneous integration, photo-detectors [2, 3], lasers [4–6], wavelength converters [7–9], and modulators [10, 11] have been shown. Modulators based on the free-carrier plasma-dispersion effect, either formed as a disk [10], [12], a ring [13], or a Mach-Zehnder interferometer [14], have attracted much interest. Other modulators are based on the Franz-Keldysh effect in strained SiGe [15, 16]. Since the electro absorption obtained by the quantum-confined Stark effect (QCSE) of InP-based multi quantum wells (MQWs) is higher than that of SiGe based MQW materials, we investigated former material system more closely.

In this paper, we report on the performance of InP microdisk modulators in carrier depletion operation regime, which have been heterogeneously integrated on a SOI waveguide. We demonstrate high-speed operation of the device with a bit-error rate below 1×10^{-9} at data rates of 2.5 Gb/s, 5.0 Gb/s and 10 Gb/s. We compare the performance of the InP microdisk modulators with a commercial lithium niobate modulator. Power penalties are presented and discussed. Finally, the power consumption is calculated and compared with that of state-of-the-art integrated modulators.

2. InP microdisk modulators

The InP microdisk modulator has been fabricated using the heterogeneous integration platform [1]. First, the silicon photonic waveguide circuitry including waveguides and grating couplers is fabricated on a silicon-on-insulator (SOI) wafer using 248 nm DUV lithography [17]. On an InP wafer a multiple quantum well (MQW) structure is grown as shown in Table 1. The MQW structure is formed by three InAsP quantum wells with a PL emission at 1520 nm embedded in non-intentionally doped (nid) quaternary InGaAsP material with a band gap of 1.2 eV. The layer stack also comprises a tunnel junction that allows for only one metallization step to contact both n -contacts of the device [18]. Then, a divinylsiloxane-bis-benzocyclobutene (DVS-BCB) adhesive was spun on top of the SOI substrate onto which a piece of the InP wafer was bonded. Subsequently, the InP substrate is removed chemo-mechanically and the device is structured using optical lithography and dry etching. We use a silicon dioxide over-cladding of the device to improve its heat-sinking. The metallization is realized by lift-off and titanium-platinum-gold (TPA) contacts. Figure 1(a) displays the schematic device structure after completion all fabrication steps. An optical microscope image made before the final pad metallization is shown in Fig. 1(b). The diameter of the active region, i.e. the MQW disk structure, is 8 μm resulting in an active area of only 50 μm^2 . When light is injected into the waveguide one of the resonance wavelengths, it can couple to the whispering-gallery modes of the disk. The light can either be modulated by changing either the resonance wavelength of the device using the free-carrier plasma-dispersion effect [10] or by changing the absorption properties of the disk, as we will show below.

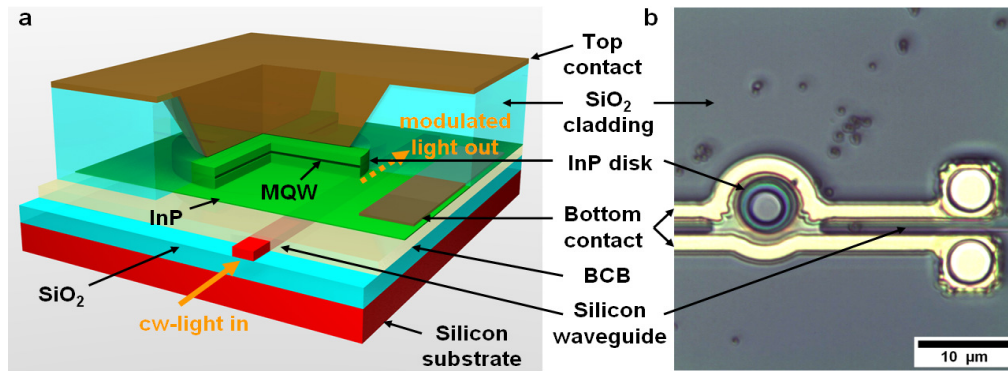


Fig. 1. Device structure of an InP microdisk modulator heterogeneously integrated on a SOI waveguide. a) Schematic view of the final device including the final metallization. b) Optical microscope image of the InP microdisk modulator before the final pad metallization.

Table 1. Epitaxial Layer Stack of the InP Microdisk Modulator

	Layer	Material composition	Doping (cm^{-3})	Thickness (nm)
1	Top contact	InP	n^+ , $1 \times 10^{18} - 5 \times 10^{18}$	80
2	Tunnel junction	Q1.3 (InGaAsP)	n^{++} , 1×10^{19} p^{++} , 2×10^{19}	20
3	Doped barrier	InP	p , $5 \times 10^{17} - 1 \times 10^{18}$	135
4	Barrier	Q1.2 (InGaAsP)	nid	25
5	QW barrier	Q1.2 (InGaAsP)	nid	15 ($\times 3$)
6	Quantum well	InAsP (1.52 μm)	nid	6 ($\times 3$)
7	Barrier	Q1.2 (InGaAsP)	nid	25
8	Doped barrier	Q1.2 (InGaAsP)	n , 1×10^{18}	120
9	Bottom contact	InP	n^{++} , 5×10^{18}	95

3. Measurements

3.1 Static characteristics

The characterization was performed on a custom-made apparatus with automatically aligned fiber probes for coupling to the SOI grating couplers on the chip. For basic device characterization, the I - V curves of more than 30 devices on the same chip were measured (Fig. 2(a)). When biasing the device in forward direction, it is electrically pumped and the device starts to emit light [4]. Below the lasing threshold the devices can also be used as a carrier-injection-based modulator [10]. Instead of positive bias, here we are interested in the negative bias regime. Leakage currents lower than $1\ \mu\text{A}$ are sustained for voltages larger than $-4\ \text{V}$. By biasing the device negatively, the quantum-confined stark effect (QCSE) modulates the absorption [11]. Although the device consists of the same epitaxial material used for lasing, the enhancement of the absorption due to the resonant cavity is sufficient to demonstrate the modulation of light. Therefore, processing steps to reduce the band gap of the quantum well, such as quantum-well-intermixing, are not required when co-integrating the modulator with a laser [19]. As operation point for the experiments we chose $1555.8\ \text{nm}$. Starting from a pre-bias of $-1\ \text{V}$ the transmission drops by $4.5\ \text{dB}$ with a voltage swing of only $2.0\ \text{Vpp}$ as displayed in Fig. 2(b). When biasing the device at $-5\ \text{V}$ more than $6\ \text{dB}$ extinction can be achieved. To demonstrate that the modulator could be directly driven by co-integrated electronics we limited the voltage swing to $2.0\ \text{Vpp}$, which is supported by state-of-the-art BiCMOS technologies commonly used for high-speed optoelectronic circuits [20]. At $1555.8\ \text{nm}$, the additional loss caused by the modulator compared with the off-resonance transmission of the waveguide is only $0.75\ \text{dB}$ as shown in Fig. 2(b).

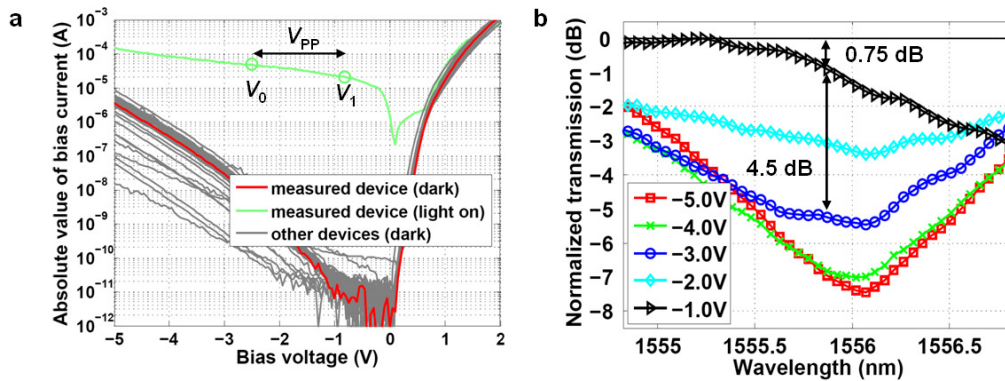


Fig. 2. a) Static electrical characteristics of the InP microdisk modulator with and without light in the waveguide. The image also displays the dark IV-curves for more than 30 devices on the same chip. b) Static optical characteristics of the InP microdisk modulator. Transmission characteristics of one device for several negative bias voltages.

3.2 Dynamic characteristics

Dynamic measurements were performed to investigate the electro-optic modulation behavior of the modulator. The measurement apparatus is depicted in Fig. 3. The sample was mounted on a thermo-electric cooler (TEC) to stabilize the device temperature at 20°C . Light from a tunable laser was fed into a polarization controller (PC) and injected into the chip by grating couplers using a cleaved single-mode fiber. This resulted in $-10\ \text{dBm}$ optical power in the silicon waveguide. A radio-frequency (RF) probe was connected to the device and directly driven by a $12.5\ \text{Gb/s}$ pulse pattern generator. The light was then coupled out off the chip by a second grating coupler and amplified by about $30\ \text{dB}$ using an erbium-doped fiber amplifier (EDFA). To measure optical eye diagrams, the light was spectrally filtered using a tunable filter with an insertion loss of $5\ \text{dB}$ and a $3\ \text{dB}$ -bandwidth of $0.25\ \text{nm}$, and monitored by a high-speed oscilloscope. For measuring BER traces the signal was fed into a variable optical

attenuator (VOA), launched into an ac-coupled 10 Gb/s photo receiver and electrically amplified. The electrical signal was then analyzed in a 12.5 Gb/s error detector, which was synchronized with the pulse pattern generator, or monitored in the oscilloscope.

The reference measurements were made with a commercial 40 Gb/s lithium niobate (LiNO₃) modulator. The optical signal was attenuated to obtain the same power at the input of the EDFA as with the InP microdisk modulator to account for the amplifier noise and evaluate the actual modulator performance.

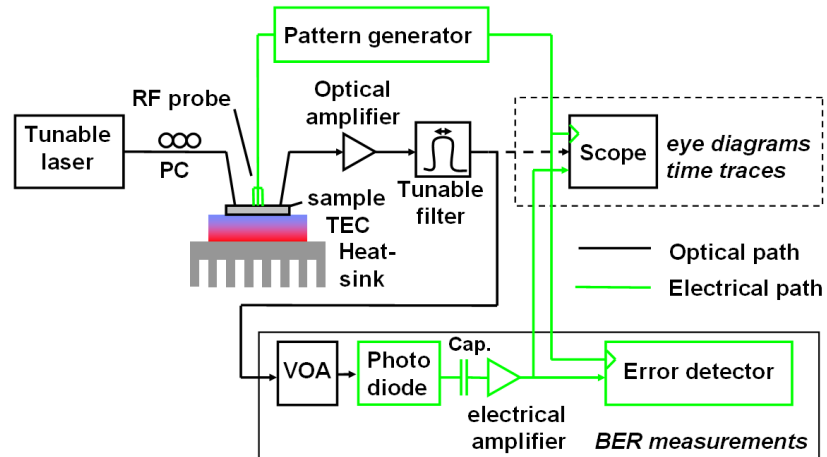


Fig. 3. Measurement apparatus for high-speed measurements (eye diagrams and bit-error rate test).

The operation wavelength was set to 1555.82 nm for all measurements. The InP microdisk modulator was driven with a one-drive-level of $V_1 = -0.875V$ and a zero level of $V_0 = -2.5V$, resulting in a peak-to-peak swing of $V_{pp} = 1.625V$. Figure 4 displays eye diagrams for the InP microdisk modulator at 2.5 Gb/s (Fig. 4(a)), 5.0 Gb/s (Fig. 4(b)) and 10 Gb/s (Fig. 4(c)) for non-return-to-zero (NRZ) pseudo-random binary sequence (PRBS) lengths of $2^{31} - 1$. As can be seen from Figs. 4(a) and 4(b), the extinction ratio of the InP microdisk modulator was about 4.5 dB for 2.5 Gb/s and 5.0 Gb/s. For 10 Gb/s the extinction ratio degraded to 2.2 dB as shown in Fig. 4(c). However, by ac-coupling the photo receiver, the offset was removed, resulting in a clear open eye at 10 Gb/s as evident in Fig. 4(d).

The speed limitations of the device originate from the electrical parasitics and are not fundamental to the absorption mechanism [21]. We have measured a small-signal 3dB-bandwidth larger than 16 GHz, which is governed by the parasitics of the device. Reducing these parasitics would improve the device speed further to allow for operation at 20 Gb/s and beyond. However, small-signal measurements only give a rough indication about the large-signal behavior of the device.

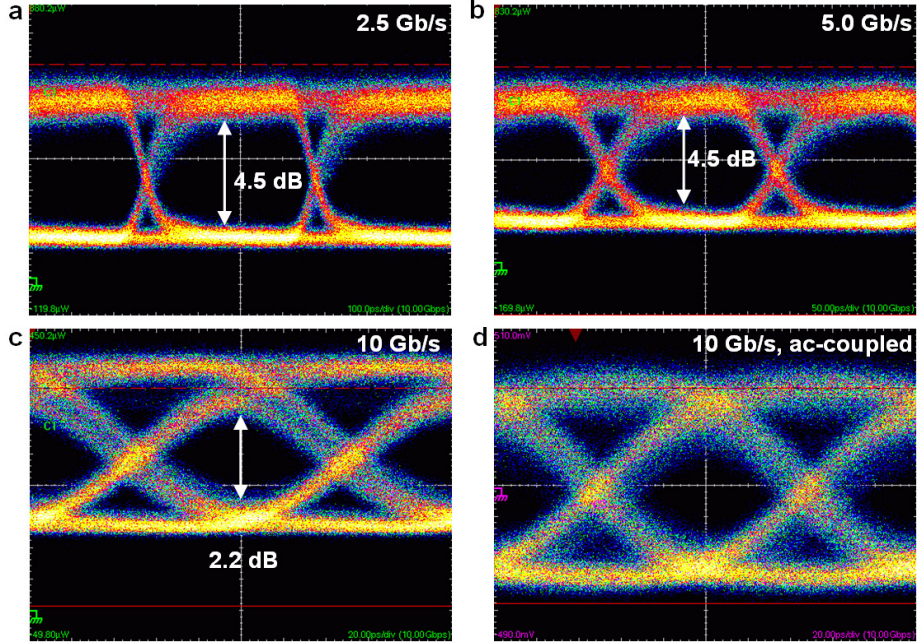


Fig. 4. Optical eye diagrams of InP microdisk modulator: a) at a bit rate of 2.5 Gb/s, b) at a bit rate of 5.0 Gb/s, c) at a bit rate of 10 Gb/s, and d) electrical eye at a bit rate of 10 Gb/s and using an ac-coupled photo receiver.

Therefore, we performed BER measurements to quantify the actual quality of the modulated optical signal. The measurements were carried out at 2.5 Gb/s, 5.0 Gb/s and 10 Gb/s and NRZ PRBS lengths of $2^7 - 1$ and $2^{31} - 1$. Error-free operation ($< 1 \times 10^{-11}$) was achieved for 2.5 and 5.0 Gb/s at a PRBS length of $2^{31} - 1$ as shown in Fig. 5(a). The power penalty compared with the commercial modulator at 2.5 Gb/s and 5.0 Gb/s was 3.1 dB and is caused by the limited extinction ratio, that can be approximated as [22]

$$P_{dB} \approx 10 \cdot \log \left(\frac{ER_{lim} + 1}{ER_{lim} - 1} \right). \quad (1)$$

For 10 Gb/s the penalty slightly increases to 4.7 dB for a pattern length of $2^7 - 1$ due to the limited extinction ratio of 3.2 dB as evident from Fig. 5(b). At a PRBS length of $2^{31} - 1$, pattern effects are limiting the extinction ratio to 2.2 dB as indicated in Fig. 5(c), resulting in an increased power penalty of 7.0 dB (Fig. 5(a)). Still, a BER lower than 1×10^{-9} could be achieved for that pattern length. This means that although the modulator exhibits a relatively limited extinction ratio we have successfully demonstrated error-free operation at 2.5, 5.0 and 10 Gb/s. The implications of the limited extinction ratio are only an increased power penalty with respect to a modulator with a large extinction ratio. Consequently, a higher laser power would be required in an optical link to obtain the required receiver power to recover the signal error-free. Therefore, it is desirable to improve the extinction ratio to obtain a low-power optical link.

During all measurement an optical signal to noise ratio (OSNR) larger than 25 dB is sustained, thus its contribution to the power penalty is not significant. Note that, because of the attenuation of the optical signal and the use of the EDFA, the commercial modulator also requires more than -10 dBm received power at the photo receiver to recover the signal without errors. Without attenuation and successive amplification, a receiver power of -19 dBm was required to obtain error-free operation with the modulator, which is consistent with the datasheet of the photo receiver (not shown in Fig. 5(a)).

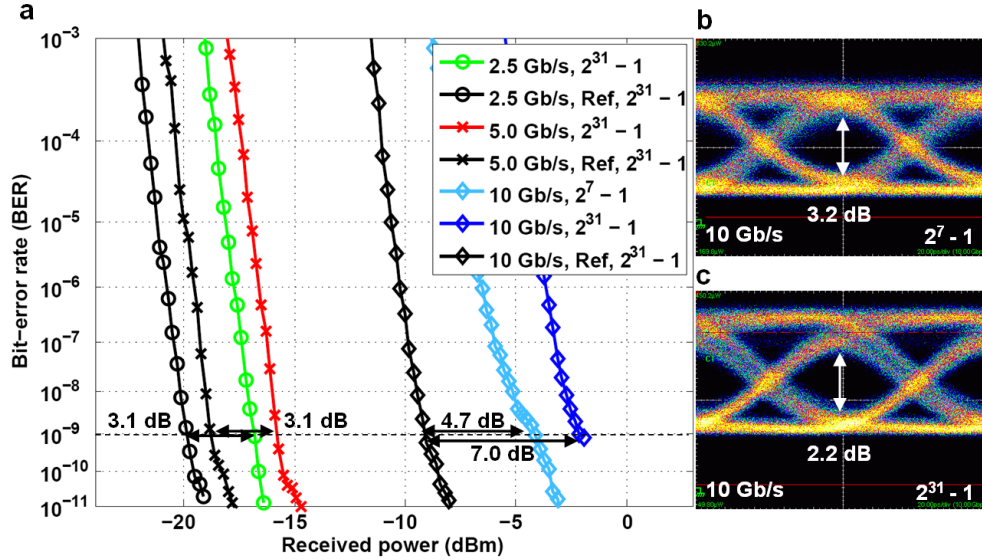


Fig. 5. a) Bit-error rate measurements of the InP microdisk modulator and a commercial modulator with bit rates of 2.5, 5.0 and 10.0 Gb/s. Eye diagrams for operation at 10 Gb/s and b) a PRBS length of $2^7 - 1$ c) a PRBS length of $2^{31} - 1$.

3.3 Power consumption

The power consumption of a modulator is predominated by ohmic losses and capacitive losses. Typically, in forward-biased devices, which are based on carrier injection, the energy consumption is predominated by the injected current [14]. However, as we use a negative drive, the junctions are reversely biased and the ohmic losses are reduced significantly. The drive current at the one drive level $V_1 = -0.875$ V is $I_1 = 2.1 \times 10^{-5}$ A, and at the zero level of $V_0 = -2.5$ V it is $I_0 = 4.6 \times 10^{-5}$ A (Fig. 2(a)). Consequently the energy consumption per bit is

$$E_{bit,curr} = 0.5 \cdot [I_1 V_1 + I_0 V_0] / BR = 7 \text{ fJ / bit.} \quad (2)$$

Note that we measured the static currents with the light in the waveguide thus including the photocurrent, which is generated in the device. In the reverse biased device, the main source of power consumption is energy to charge and discharge the active region capacitance. Fitting the S_{11} parameters with a small-signal equivalent circuit up to 40 GHz, a capacitance of the active region of $C_a = 54.7$ fF has been extracted. A simple plate capacitor model with a distance of the total undoped layer thicknesses of 113 nm resulted in a capacitance of $C_a' = 43$ fF, which does not include fringe capacitances. The energy to charge the capacitor is $\frac{1}{2}CV^2$; for a PRBS stream it is half of that:

$$E_{bit,cap} = 0.5 \cdot \frac{1}{2} C_a V_{pp}^2 = 36 \text{ fJ / bit} \quad (3)$$

Hence, the modulator requires a total energy of only 43 fJ to process one bit at 10 Gb/s, when neglecting the power for stabilizing the resonance wavelength. Since most resonant devices are sensitive to temperature fluctuations resulting in wavelength shifts, power to keep them on-resonance is required. The tuning can be realized either by heating or by cooling. Also within heaters and coolers, several techniques exist. Also the temperature stabilization system of the laser could be shared with the modulator and also filters. Including a number for the energy consumption of the wavelength tuning system strongly depends on the application, the implementation and the system and is therefore not considered. Table 2 compares operating principle, biasing conditions, area consumption, speed, static extinction ratio, and energy consumption of several high-speed low-power modulator concepts. Extensive research efforts have reduced the energy consumption of modulators from 5 pJ/bit [14] down

to single-digit fJ/bit values [23] over the last years. While most devices suffer from limited extinction ratios [23], high drive voltages [14] and a large energy consumption [13, 14], our devices represent a good compromise. Moreover, our proof-of-concept study on InP microdisk modulators uses devices that are not fully optimized yet. Especially a reduction of the device diameter, leading to a quadratic reduction of the capacitance, is expected to deliver even higher speed and reduce the energy to the single-digit fJ/bit regime. Also, a reduction in the parasitic pad capacitances is expected to increase the device speed while lowering the total energy consumption leading to ultra-low power high-speed modulators.

Table 2. Comparison of the Present Work with State-of-the-Art Modulators in Terms of Drive Voltage, Area, Speed, Static Extinction Ratio and Energy Consumption per Bit [23].

Publication	Year	Type	V _{pp}	Area	Speed	Static Ext-R	Energy
Green <i>et al.</i> [14]	2007	MZM	7.6 V	1000 μm^2	10.0 Gb/s	6 dB	5 pJ/bit
Xu <i>et al.</i> [13]	2007	Ring	3.5 V	310 μm^2	12.5 Gb/s	9 dB	300 fJ/bit
Liu <i>et al.</i> [16]	2008	EAM	3.0 V	200 μm^2	1.2 Gb/s	8 dB	50 fJ/bit
Watts <i>et al.</i> [12]	2008	Disk	3.5 V	13 μm^2	10.0 Gb/s	4.8 dB	58 fJ/bit
Dong <i>et al.</i> [24]	2009	Ring	2.0 V	1000 μm^2	11.0 GHz	6.5 dB	50 fJ/bit
Dong <i>et al.</i> [25]	2010	Ring	1.0 V	1200 μm^2	10.0 GHz	6.0 dB	10 fJ/bit
Watts <i>et al.</i> [23]	2011	Disk	1.0 V	10 μm^2	12.5 Gb/s	3.2 dB	3.0 fJ/bit
<i>This work</i>	<i>2011</i>	<i>Disk</i>	<i>1.6 V</i>	<i>50 μm^2</i>	<i>10.0 Gb/s</i>	<i>4.5 dB</i>	<i>43 fJ/bit</i>

4. Conclusion

We have demonstrated the modulation characteristics of a reversely biased InP microdisk modulator heterogeneously integrated on top of an SOI waveguide. We presented static extinction ratios of 4.5 dB for a bias swing of only 2.0 V_{pp}. To investigate the application in a system context, we measured bit-error rates at 2.5 Gb/s, 5.0 Gb/s and 10.0 Gb/s. For speeds up to 10 Gb/s, we successfully demonstrated operation with a BER lower than 1×10^{-9} . We analyzed the performance of a commercial modulator and found power penalties of about 3.1 dB for 2.5 Gb/s and 5 Gb/s due to the limited extinction ratio. For 10 Gb/s the power penalty was found to be 4.7 dB for a pattern length of $2^7 - 1$, whereas for $2^{31} - 1$ the penalty was 7.0 dB. The reduced extinction ratio at high speed and long patterns was found to be the main source of the power penalty.

The work presented here demonstrates the applicability of InP microdisks as high-speed electro absorption modulators with in the carrier depletion operation regime. Drive voltages of less than 2.0 V_{pp} can easily be achieved by state-of-the-art BiCMOS technologies. The energy consumption of 43 fJ/bit of our device is comparable to fully optimized state-of-the-art modulators. The device combines low footprint and high operation speed. This together with the possibility of co-integrating lasers, wavelength converters and detectors using the same epitaxial material and the same processing scheme, make the presented modulator very attractive for integrated photonics.

Acknowledgments

This work was supported by the European Union FP7-ICT project "HISTORIC". The authors acknowledge fruitful discussions with F. Horst and S. Abel, and technical support by H. Steinauer (IBM).